

4 The Si(100)-c(4x2) Surface

The electronic and geometric structures of silicon are well known as it is one of the most studied materials in solid state physics. The basic reconstruction mechanism of the Si(100) surface is dimerization. The ground state of the geometric structure of the surface is a $c(4 \times 2)$ buckled dimer reconstruction proposed by Chadi already in 1979 [Cha79]. The electronic structure has been in detail investigated by two-photon photoemission (2PPE). In this chapter I will outline the interplay of the electronic and geometric structure of the Si(100) surface. Electron dynamics occurs on the picosecond time-scale and coupling of electronic to vibronic excitations has been probed in a two-color two-photon photoemission (2C-2PPE) experiment combining synchrotron and laser excitation.

4.1 Bulk Properties

4.1.1 Band Gap

Silicon is one of the most used substrate materials and is nowadays very important for device technology. It is an element of the fourth group and crystallizes in the diamond structure with a lattice constant of 5.4 Å [Kit93]. Clean silicon is a semiconductor and has at room temperature an indirect band gap E_G of 1.17 eV. The energy band gap of silicon decreases with increasing temperature. The thermal expansion of the material, i.e. the increased interatomic spacing, reduces the splitting between occupied and unoccupied states and thus the size of the band gap. The temperature dependence of the silicon band gap has been experimentally determined and is described by the following equation:

$$E_G = 1.17 \text{ eV} - \frac{\alpha T^2}{T + \beta} \quad (4.1)$$

where $\alpha = 4.73 \cdot 10^{-4}$ eV/K and $\beta = 636$ K [htta]. In a linear approximation at $T = 300$ K the band gap energy can be written as $E_G = 1.17 \text{ eV} - 0.25 \text{ meV/K} \cdot \Delta T$, where $\Delta T = T - 300$ K. A temperature increase of $\Delta T = 100$ K reduces the indirect band gap by approximately 25 meV. The direct band gap of silicon is 3.4 eV at the Γ -point and thus clearly bigger.

4.1.2 Optical Penetration Depth

The indirect band gap of silicon determines the light absorption in the spectral range below 3.4 eV. Figure 4.1 shows the optical absorption of silicon as a function of photon energy for different temperatures. The linear absorption coefficient α enters the absorption law:

$$I(l) = I_0 e^{-\alpha l} \quad (4.2)$$

where I is the light intensity as a function of penetration depth l into the crystal. When the intensity of the light decreases to $1/e$, it is most easy to calculate the absorption length by $l_\alpha = \alpha^{-1}$. In this work a photon energy of 1.56 eV is used, which corresponds to an absorption length of approximately $10 \mu\text{m}$.

4.1.3 Doped Semiconductor

Even nowadays, the purest silicon crystals have a density of about 10^{12} of intrinsic impurities per cubic centimeter. The optical properties are little influenced by doping but the electronic properties change strongly, because by doping free carriers are generated in the semiconductor.

The silicon experiments presented in this work were performed using a p-doped silicon crystal and a (100)-oriented surface. The doping concentration p_o is $10^{15}/\text{cm}^3$ resulting in a specific resistance of $10 \Omega \cdot \text{cm}$. The Debye length is the distance over which the mobile carriers screen out electric fields in semiconductors. The Debye length is an important parameter for the study of surface photovoltage in semiconductors. It can be written as

$$\lambda_D = \sqrt{\frac{2k_B T \epsilon_r \epsilon_0}{e^2 p_0}} \quad (4.3)$$

hence, at room temperature, the Debye length in silicon is $\lambda_D = 0.18 \mu\text{m}$, with, $\epsilon_r = 11.8$.

4.2 Geometric and Electronic Structure of Si(100)

As mentioned before, silicon is an element of the fourth group and crystallizes in the diamond structure. In a silicon single-crystal each silicon atom forms four covalent bonds in tetrahedral configuration with its neighbors. Figure 4.2 displays the crystal unit-cell with an unreconstructed (100) surface. Silicon atoms at the surface exhibit two unsaturated bonds, *dangling bonds*. As a result of minimization of the surface energy two adjacent surface atoms form a dimer. The direction of the dimerization is predetermined by the orientation of the dangling bonds. By dimerization

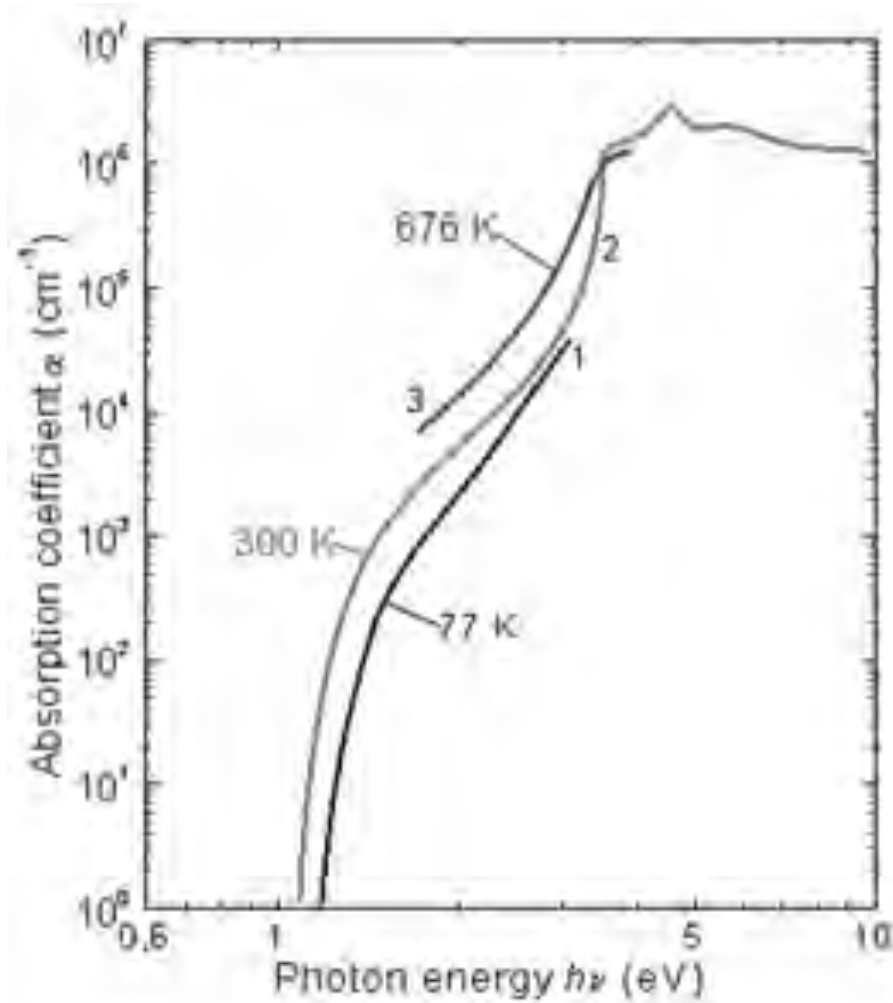


Figure 4.1: Absorption coefficient of silicon versus photon energy for different temperatures, reproduced from Refs. [Jel82, Sze81].

the number of unsaturated bonds is reduced to one half and the surface unit cell is doubled in the direction of the dimer axis forming a (2×1) reconstruction. The latter was first observed by *Schlier and Farnsworth* (1959) [Sch59].

Details of the reconstructions are schematically summarized in Fig. 4.3. The (2×1) reconstruction has 1.7 eV less energy per dimer compared to the unreconstructed (1×1) surface [Mön95]. The energy gain of an asymmetric dimer reconstruction compared to the symmetric dimer configuration is 0.1 eV per dimer [Krü95, Dab92]. Low-energy electron diffraction (LEED) [Yan83, Hol84] and X-ray diffraction (XRD) [Jed90] as well as diffraction of Helium-atoms [Aon82] confirm this asymmetric dimer model for the (2×1) reconstructed Si(100) surface. The dimers

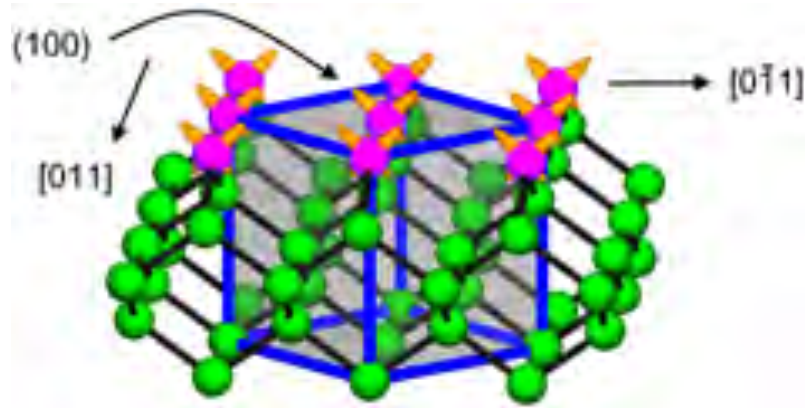


Figure 4.2: Section of a silicon crystal with cubic unit cell and unreconstructed (100) surface. The atoms at the surface exhibit two unsaturated bonds. Reproduced from [Fin01].

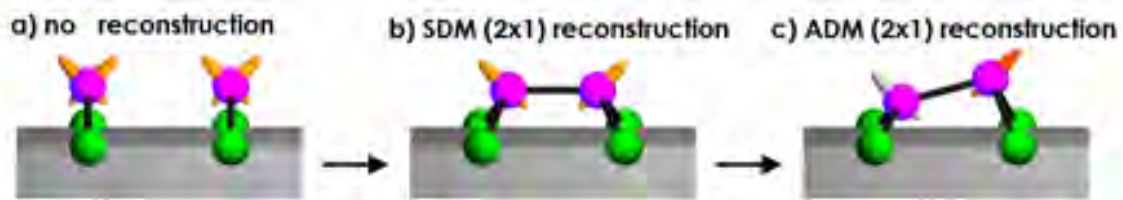


Figure 4.3: Surface reconstruction of Si(100)-surface. Symmetric dimer model (SDM) and asymmetric dimer model (ADM). Reproduced from [Fin01].

are tilted by 8° with respect to the (100) surface. Such distortions are accompanied by rehybridization of the surface bonds and, as a consequence, a rearrangement of surface charges. A threefold coordinated surface atom, which is depressed inward, will change its back bond towards more sp^2 -like so that its dangling bond D_{down} will become more p_z -like. The other surface atom moves outward. It will exhibit back bonds of more p -like character while its dangling bond D_{up} will tend towards more s -like character. As a consequence of such rehybridization, charge is transferred from D_{down} to D_{up} dimer atom. The D_{up} band becomes completely filled, while the D_{down} band is empty. Table 4.1 displays the structural parameters for the Si(100) surface.

(2 × 2) and c(4 × 2) Reconstruction

At room temperature the Si(100) surface exhibits a (2 × 1) LEED pattern, while at 90 K two different configurations of c(4 × 2) and of p(2 × 2) periodicity are observed. The structural transition takes place at 220 K [Tab87]. Figure 4.4 displays the different reconstructions at low temperature. The two reconstructions only differ with respect to the orientation of the asymmetric dimer [Nor93, Hea01]. According to density

Parameter	Si(100)
Lattice constant	5.43 Å [Ash76]
Binding length	2.35 Å
(2 × 1) unit cell	7.68 × 3.84 Å
Dimer length	2.24 ± 0.08 Å [Ove97]

Table 4.1: Experimental and theoretical structural parameters for Si(100) surface [Fin01].

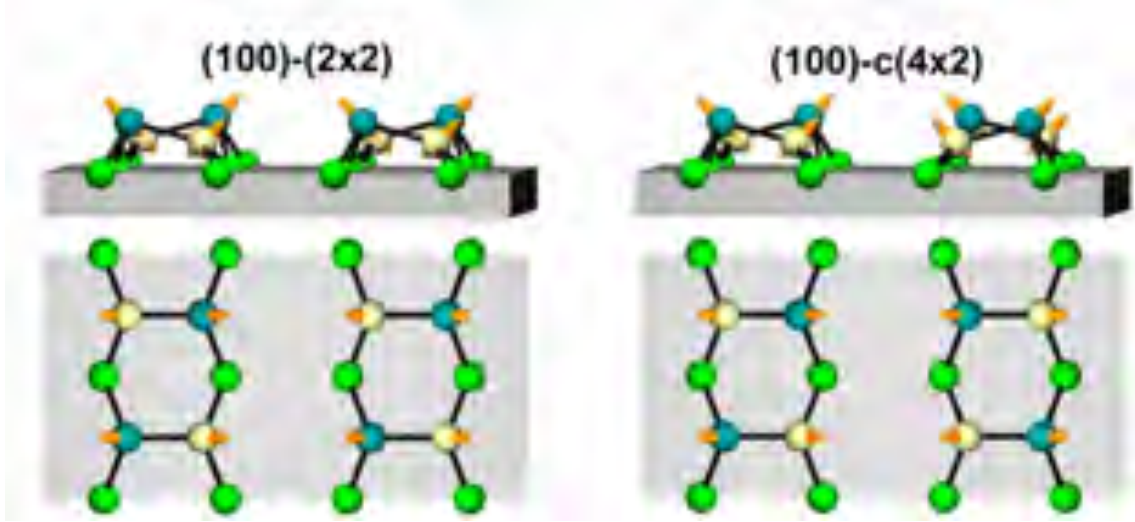


Figure 4.4: (2 × 2) and c(4 × 2) reconstructed surface by low temperatures. The dimer atoms, which are displaced inward, are lighter colored. Recorded from [Fin01].

functional theory the energetic favorable reconstruction is the c(4 × 2) periodicity. The c(4 × 2) reconstruction of the Si(100) surface consists of four dangling bonds per unit cell, because the unit cell is doubled. As a consequence the surface band structure is made up of two occupied and two unoccupied bands, i.e. each band splits in two new states (Fig. 4.5).

Electronic Structure of the Si(100) Surface

The electronic structure of the clean Si(100)(2 × 1) surface has been investigated by theoretical and by experimental studies since the eighties, some examples are in the following references [Uhr81, Far84, Him85, Gol86, Cha79, Asa00]. The structure for Si(100) c(4 × 2) is shown in Fig. 4.5. The grey shaded areas correspond to the surface-projected bulk bands. Occupied and unoccupied dangling-band are labeled D_{up} and D_{down} . The surface band-gap of Si(100) was found to be ≈ 0.81 eV [Ken01]. The pump-line pulse photon energy used in the present experiment is 1.56 eV. Therefore electrons from the occupied surface dangling-bond band can be

excited into the unoccupied band in an one-photon absorption process. Excitation between bulk states requires at least a two-photon absorption process, because the direct gap of silicon is about 3.4 eV.

Measurements were performed on a two-domain surface. In the following **even**

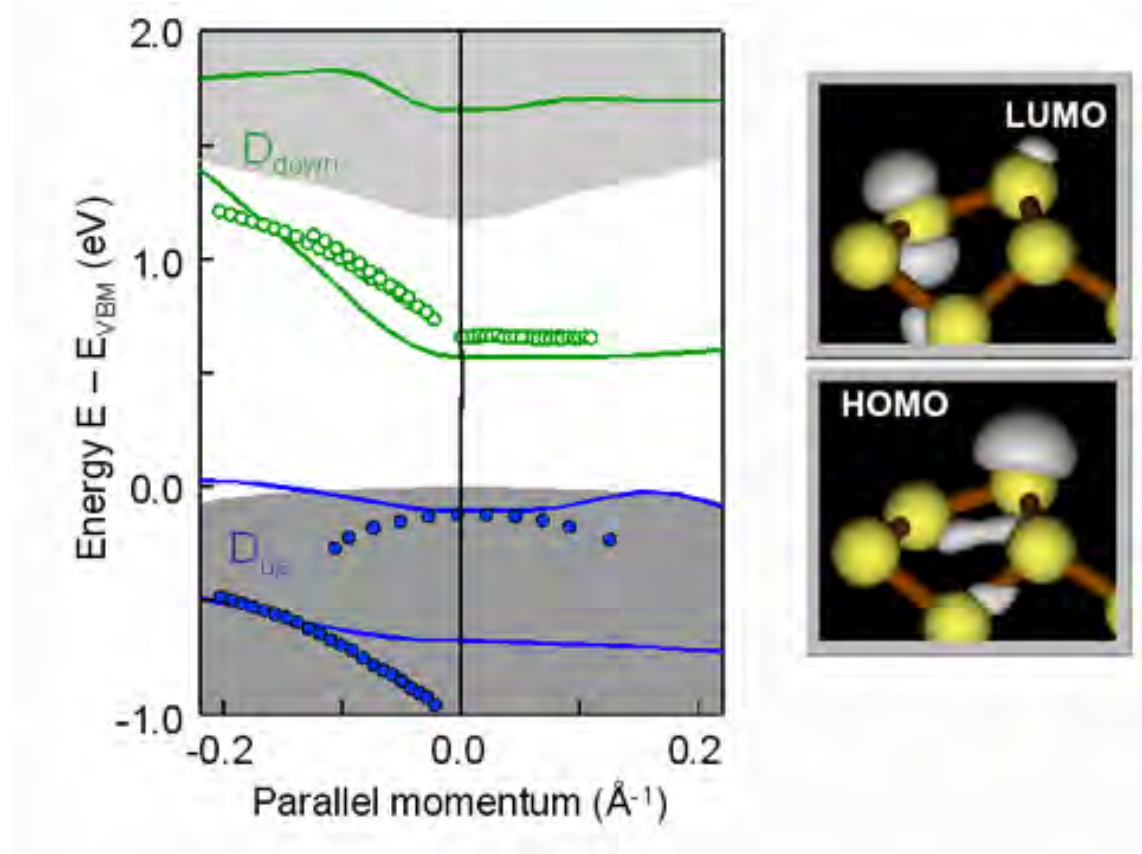


Figure 4.5: a) Surface-projected band-structure of Si(100)(2×1) for asymmetric dimers with the unoccupied (D_{down}) and occupied (D_{up}) surface bands [Wei05]. The grey zone displays the projection of the bulk bands. b) Charge density of the silicon dimers upon laser excitation [Nor93].

symmetry denotes the situation where the polarization of the synchrotron light is parallel to the detector, while **odd** symmetry corresponds to a measurement geometry where the light polarization is perpendicular to the detector. The energy spectra scale of the photoemission in this chapter are aligned assuming that the D_{up} dangling-bond band is located at 0.7 eV below E_F [Ken01], the Si $2p_{1/2}$ core-level at 99.8 eV and the Si $2p_{3/2}$ core-level at 99.2 eV [httb].

The dangling-bond states are much clearer identified recording angle-resolved photoemission spectra. Fig. 4.6 shows angle-resolved photoemission spectra for the clean Si(100)-(4×2) surface in the even geometry. The plane of detection is oriented along

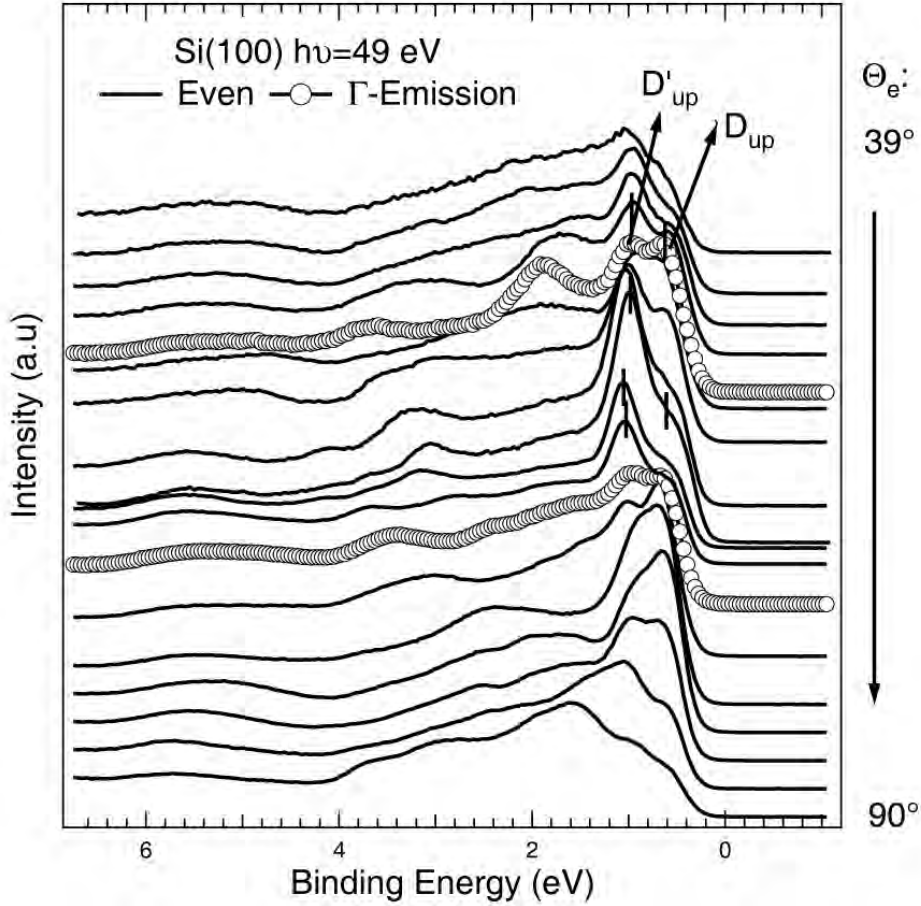


Figure 4.6: Angle-resolved ultraviolet photoemission (ARUP) spectra of the clean Si(100)-(4 × 2) surface, recorded at a photon energy of 49 eV, and for different emission angles (Θ_e). Emission at $\bar{\Gamma}$ is highlighted with circles and peak positions of the dimer band and the dangling-bonds are marked by lines.

the $[0\bar{1}1]$ -direction. The emission angles change between $\Theta_e=39^\circ$ and 90° in steps of 3° . Spectra with emission angles corresponding to the $\bar{\Gamma}$ point of the Brillouin zone are highlighted with circles. Vertical bars mark peaks attributed to the dangling bond bands.

4.2.1 Preparation of the Si(100) Surface

Samples were cut from a $\langle 100 \rangle$ oriented p-doped wafer ($\rho = 10 \Omega cm$). The wafer has at the surface a native oxide layer of approximately 2 to 3 μm thickness which isolates the semiconductor from environmental influences. There are different procedures to remove the oxide from the Si(100) surface. We used the following: the crystal was annealed for 12 hours at 800 K. By this procedure, sample and sam-

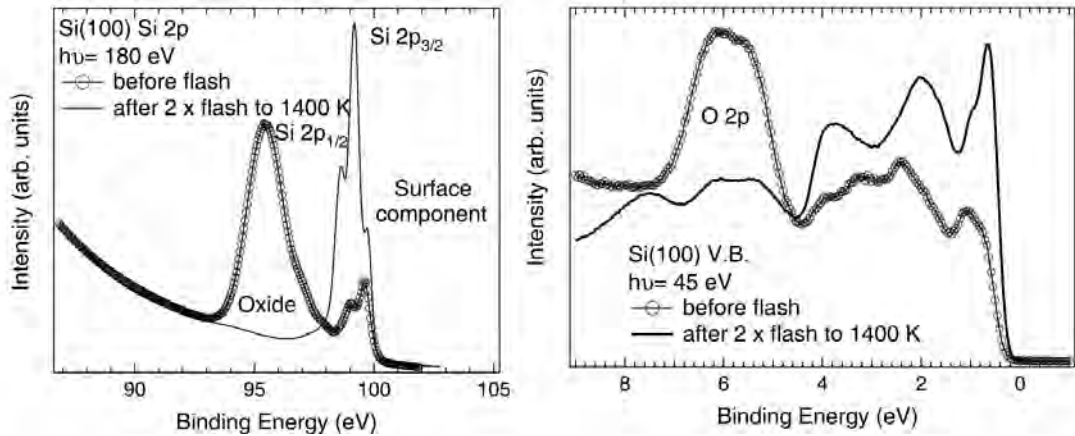


Figure 4.7: a) Photoemission spectra of the valence-band of Si(100) surface recorded in odd geometry, before and after flashing the sample. b) Photoemission spectra of Si 2p core-level recorded in odd geometry, before and after flashing the sample.

ple holder are degassed. Until the pressure remains below 10^{-10} mbar. Afterwards the silicon sample is heated to 1400 K with the pressure staying below $1 \cdot 10^{-10}$ mbar. Figure 4.7 shows photoemission spectra in two different spectral regions for the Si(100) surface. Fig. 4.7a displays the valence-band of Si(100) recorded at a photon energy of 49 eV. Circles represent the valence-band before a flash to 1400 K, where emission from the natural oxide states occurs at 6 eV. The solid line is the valence-band spectrum after two times flashing the sample to 1400 K. The natural oxide disappears and the dimer dangling bond band becomes visible at an energy of 0.7 eV. Figure 4.7b shows the Si 2p peak of Si(100) before and after flashing, the surface Si 2p component appears after flashing the sample.

4.3 Band Bending and Surface Photovoltage

The following section outlines the fundamentals of band bending and surface photovoltage (SPV) in a p-doped silicon semiconductor. The first theoretical studies about band bending in semiconductors were published by Garrett and Brattain [Bra47, Bra53, Gar55] and led to the discovery of the transistor effect. The first experimental study of SPV was done by Johnson in 1957 [Joh58]. His work investigated the SPV for germanium samples for different doping levels as a function of the excited carrier density. For an overview about SPV phenomena see the theory and experiment of Kronik and Shapira [Kro99].

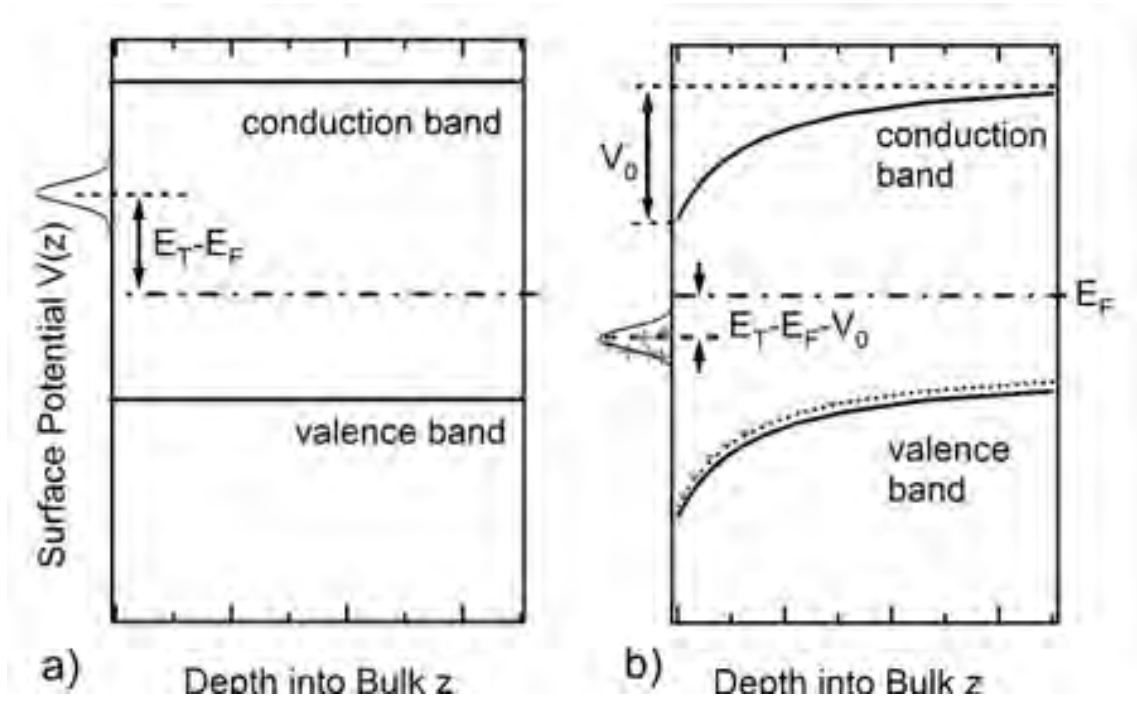


Figure 4.8: Band bending at the surface of a p-doped semiconductor. a) The theoretical situation of flat bands with a surface state acceptor relative to the valence and conduction bands. b) In equilibrium a donor state is not stable above the Fermi level.

4.3.1 Band Bending

Surface states on semiconductors can have either donor or acceptor character resulting in a net surface charge Q_{ss} states. The surface region will remain electrically neutral. This implies a space charge layer beneath the surface. Then the condition of charge neutrality is given by

$$Q_{ss} + Q_{sc} = 0 \quad (4.4)$$

where Q_{sc} is the space charge per unit surface area. The situation is illustrated in Fig. 4.8 for a p-doped semiconductor. With acceptor type surface states, when the surface state level is above the Fermi level, the bands need not to be bent, they are neutral and no space charge is required for compensation. If the bands are bent downwards (Fig. 4.8b) a negative space charge exists beneath the surface. Furthermore, the surface acceptors move closer to the Fermi level and become negatively charged. In this case, the charge in the surface state and the space charge will have the same sign, which is a violation of the condition of surface charge neutrality. In Fig. 4.8b E_T denotes the energetic position of the donor-state relative to the Fermi level and V_0 is the surface potential.

In a p-doped silicon semiconductor crystal a p_0 doping concentration of $10^{15}/\text{cm}^3$,

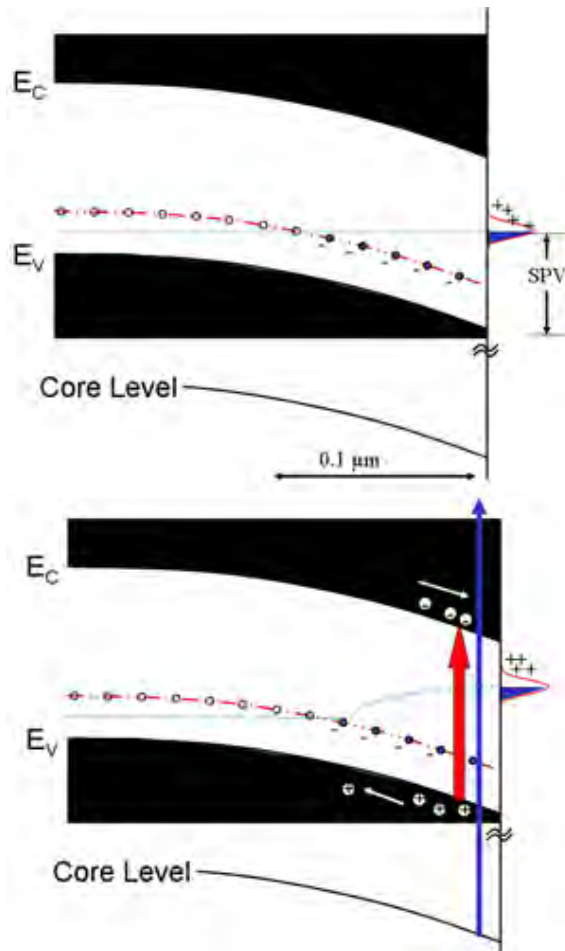


Figure 4.9: Schematic band diagram of a semiconductor. Top: Band diagram of a p-doped semiconductor with band bending. Bottom: Schematic band diagram upon laser excitation. The band bending is reduced by carriers populating the depletion zone.

the Fermi level is located 0.3 eV above the top edge of the valence-band at room temperature. Only positively charged donor levels obey the condition of charge neutrality in a p-doped semiconductor (see Fig. 4.8b). When the donor level is close to the Fermi level the density of states increases. Consequently, the equilibrium surface band-bending initially changes very rapidly but its variation then considerably slows down. The surface band-bending saturates when the Fermi level comes close to the surface state. This behavior is usually referred to as pinning of the Fermi level. It is caused by slight variations of Q_{sc} when the surface band-bending changes by a few $k_B T$, while the Fermi-Dirac distribution function, which controls the occupancy of the surface state, goes from $f_0 \approx 1$ to $f_0 \approx 0$ within approximately $2k_B T$ above and below the Fermi energy.

4.3.2 Surface Photovoltage

Generally, the photovoltaic effect is an illumination-induced change of the potential distribution in a given structure. It was discovered by Becquerel *et al.* as early as 1839 [Ngo95]. The photovoltaic effect is typically the result of some charge transfer and/or redistribution within the device due to the incident radiation. A specific variant of the photovoltaic effect is the surface photovoltage (SPV). The SPV is the change in band bending, i.e. in surface potential V_0 due to illumination-induced carriers. This effect is observed, e.g, at Si and Ge surfaces and was first reported by Brattain *et al.* in 1947 [Bra47].

Figure 4.9 displays a schematic band diagram for a p-doped semiconductor before and after laser excitation. Before laser excitation, i.e, in equilibrium the bands are bend. The extent of the space-charge region in a p-doped semiconductor is about $0.18 \mu\text{m}$, see Eq. 4.3.

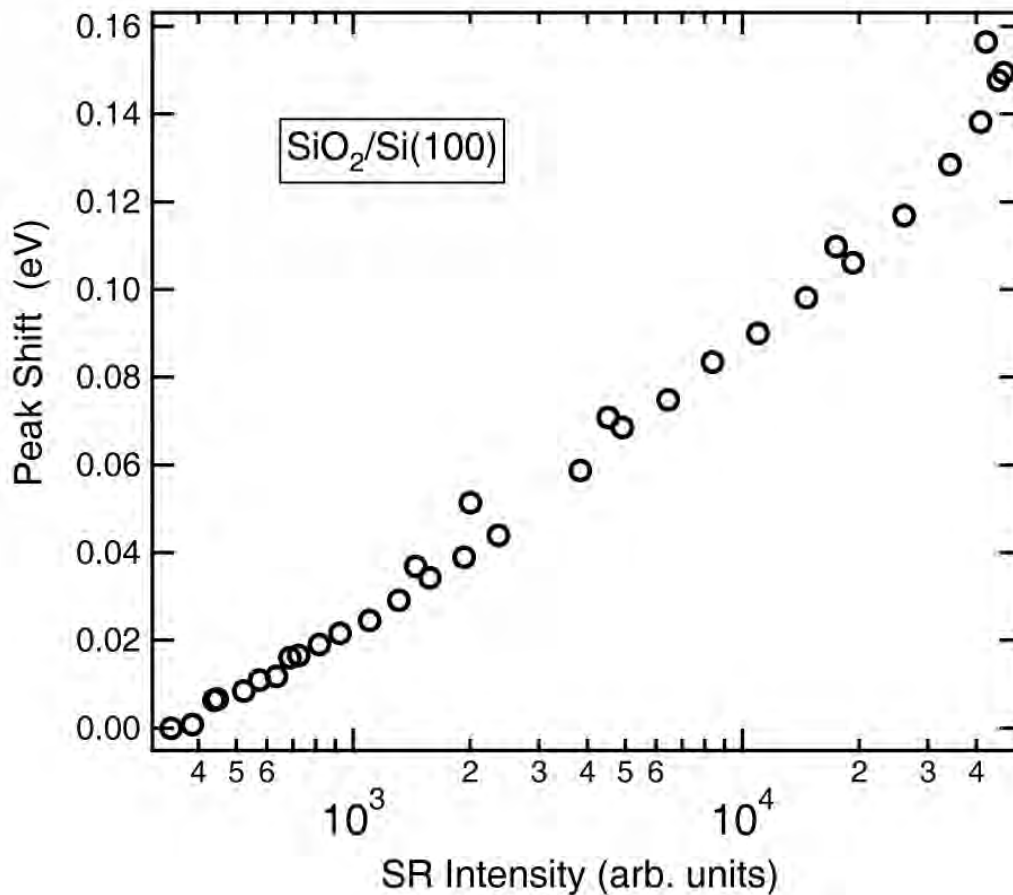


Figure 4.10: Si 2p core level shift ΔV as a function of synchrotron intensity for a 15 \AA SiO_2 layer on Si(100).

After laser excitation the band bending is reduced by optically excited carriers, increasing the population in the depletion zone. An intensive study of SPV goes beyond the scope of this work. The SPV effect at clean silicon is used in Section 2.3.2 to detect the temporal overlap between laser and synchrotron pulses, i.e, the zero of the delay time.

Surface photovoltage Induced by Synchrotron Radiation

For above band gap laser excitation ($h\nu > E_c - E_v$), also named super-bandgap illumination, the probability of band to band absorption is typically orders of magnitude larger than the probability of defect or surface states to band absorption. The illumination may change the surface potential only by the formation of electron-hole pairs.

Figure 4.10 plots the SPV induced by synchrotron radiation with an energy of 130 eV for a 15 Å silicon oxide layer on Si(100). The Si 2p core-level shifts by about 220 meV when the intensity of the synchrotron beam decreases by three orders of magnitude.

4.4 Electron Dynamics

The electronic structure and electron dynamics at the Si(100) surface are studied by two-color two-photon photoemission, combining laser and synchrotron radiation. Using synchrotron radiation the valence-band and core-levels of silicon are accessible which leads to a better understanding of the ultrafast dynamics at high excitations densities of silicon. The c(4×2) reconstruction splits into two dangling-bond states at the surface, i.e, the occupied D_{up} and the unoccupied D_{down} bands. In the following sections I will describe the response of the buckled surface dimers to the optically excited and redistributed electron population in the silicon dangling-bond bands.

4.4.1 Valence-Band and Dangling-Bond States

Numerous studies of the valence-band dynamics of Si(100) have been carried out applying two-photon photoemission experiments [Wei05, Tan03, Tab87]. They reach energetically only the valence-band region. Combining laser and synchrotron it is possible to study core-level and valence-band spectral regions. Results shown in this section have been measured at BESSY at the U125-1/PGM beamline in the low- α mode ¹ (Section 2.2.3).

When interpreting photoemission spectra from a semiconductor excited by intense laser pulses SPV and space charge effects (SCE) have to be addressed properly.

¹Operation mode, available only two weeks per year at the synchrotron facility BESSY, which has low intensity and short SR pulses width typically between 5 to 10 ps.

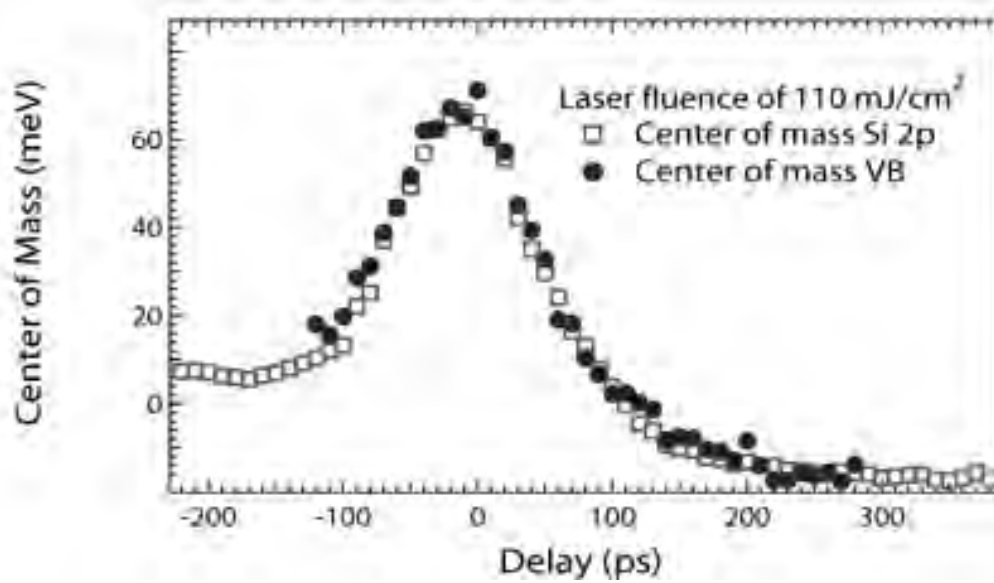


Figure 4.11: Center of mass for Si 2p and valence-band spectra.

High laser fluences up to the damage threshold have been used to separate SPV and space-charge effects from transient changes of the electronic structure induced by a femtosecond (fs) laser pulse. SPV and SCE at a certain excitation energy are characterized by a rigid shift and broadening of the whole spectrum [Pas06]. Figure 4.11 shows the center of mass for the valence-band and Si 2p spectra as a function of the time delay between the laser and synchrotron-radiation pulses. The spectral shifts of the Si 2p core-level and the valence-band are comparable for the same laser fluence of 110 mJ/cm^2 . The damage threshold of silicon was found to amount to 180 mJ/cm^2 , which is in good agreement with theoretical [Bul04, Bul05] and experimental [Jes02] studies (see Section 4.4.3).

Figure 4.12 shows a set of measurements in the valence-band region for an excitation fluence of 110 mJ/cm^2 at a photon-energy of 1.56 eV and a laser pulse width of 70 fs . The synchrotron photon-energy was 49 eV . Valence-band spectra were recorded at an emission angle of 15° with an angular acceptance of $\pm 8^\circ$. Fs-laser-pump and synchrotron-probe pulses were p-polarized with at an angle of incidence of $\sim 60^\circ$ with respect to the surface normal. The Fermi level (E_F) was determined by assuming the D_{up} at a binding energy of 0.7 eV . The laser pulse was tuned from negative delay to positive delay with respect to the synchrotron pulse. For negative delay the laser pulse arrives at the sample surface before the synchrotron radiation pulse. The data acquisition took six and a half hours. Photoemission spectra before and after the measurement showed that the Si(100) surface stayed clean during the measurement. The surface photovoltage and SCE were evaluated from Si 2p spectra recorded for identical excitation fluence. Spectra in Fig. 4.12 have been

corrected by the corresponding offset. The feature at the valence-band for negative delay (blue spectrum), is assigned to the occupied dangling-bond band D_{up} . For overlapping pump and probe pulses the intensity of the D_{up} peak decreases and a peak above the Fermi level appears, which is attributed to the transient population of the unoccupied surface band, D_{down} .

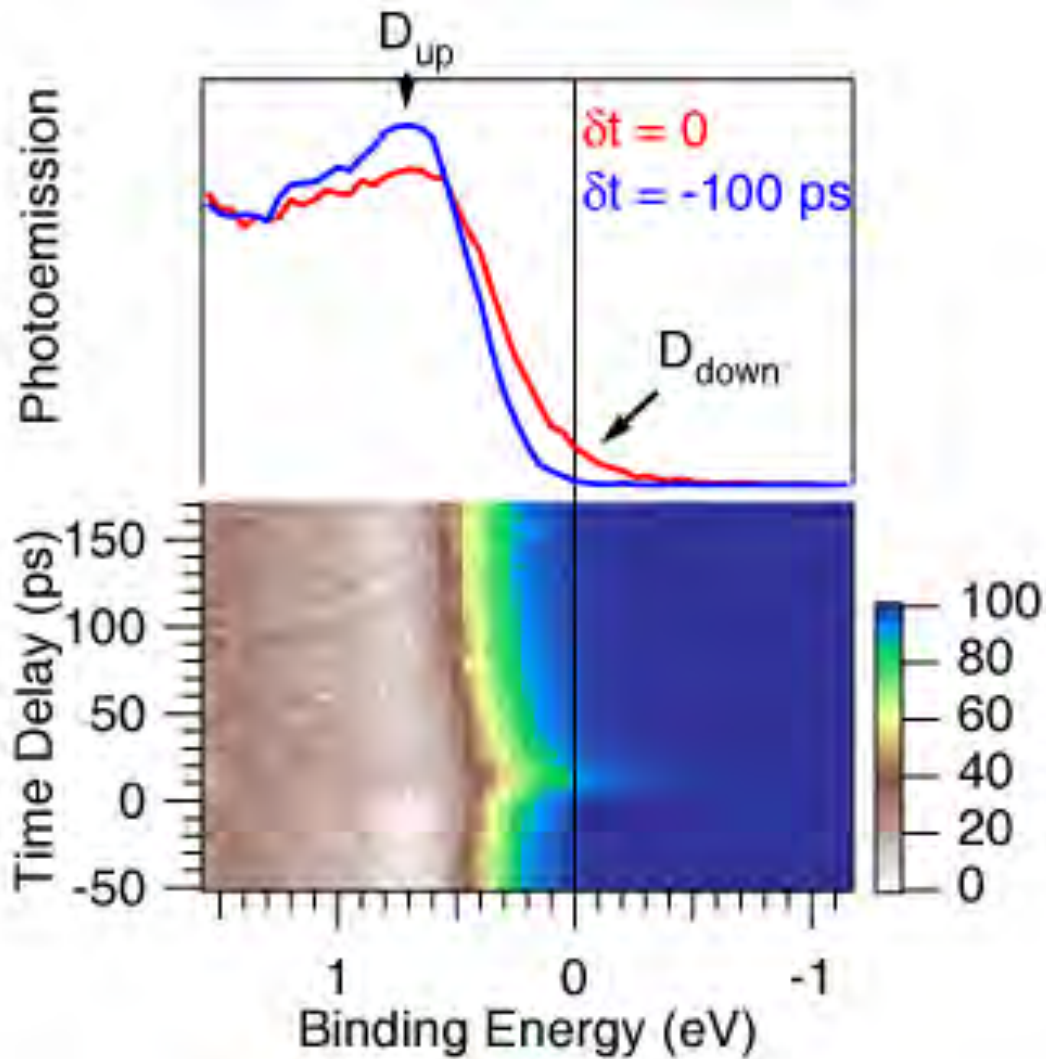


Figure 4.12: Top: Valence-band spectra recorded in the BESSY low- α mode for two different delay times between laser and synchrotron. The spectra are recorded at a photon energy of 49 eV and a laser fluence of 110 mJ/cm². Bottom: Two dimensional plot of a series of Si(100) valence-band spectra as a function of the time delay between laser and synchrotron.

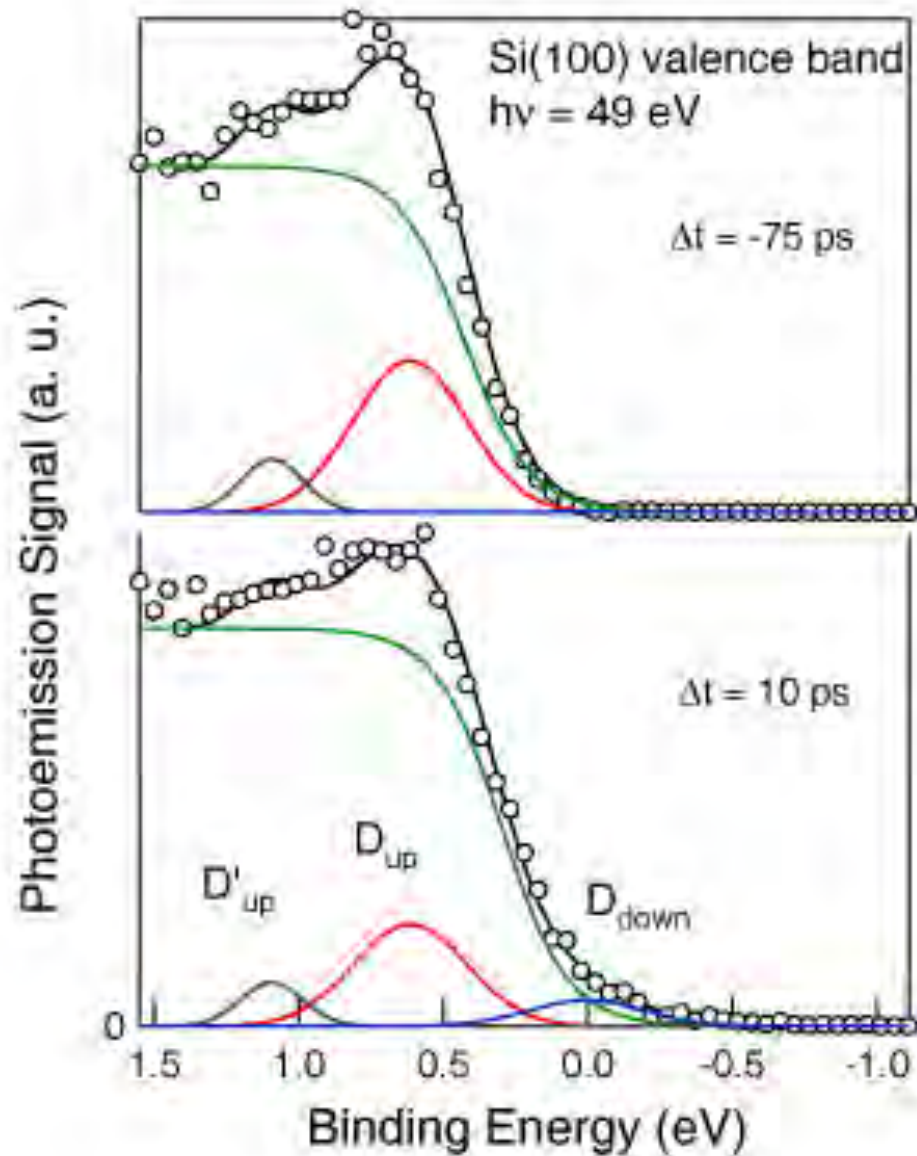


Figure 4.13: Valence-band spectra for different time delays between laser and synchrotron-radiation. Red and black Gaussian peaks represent the intensity of the occupied dangling-band states and the blue Gaussian illustrates the change in the unoccupied state. The green step function represents the valence-band of Si(100).

Surface Contribution

As illustrated in Fig. 4.13 the data from the valence-band spectra are fitted to a function composed of a broadened step function describing the bulk states, two Gaussian peak functions for the split occupied D_{up} and D'_{up} surface bands and an

additional gaussian for the lower branch of the transiently populated unoccupied D_{down} band.

The temporal evolution of the step position will be discussed in the following Section. It is attributed to a transient renormalization of the silicon bulk band-gap. The area of the two Gaussian peaks describing D_{up} and D_{down} states are plotted in Fig. 4.14 as a function of the time delay between laser and synchrotron-radiation pulses.

The increase of the D_{down} signal upon laser excitation is compatible with the decrease of the D_{up} signal. Furthermore, the subsequent relaxation follows the same temporal evolution. The decrease of the D_{up} signal correspond to a depopulation of the occupied surface band by about 40%. Thus for a fluence of 110 mJ/cm^2 nearly each dimer is excited. For a depopulation of 40%, and a density of dimers of $7 \cdot 10^{14}$

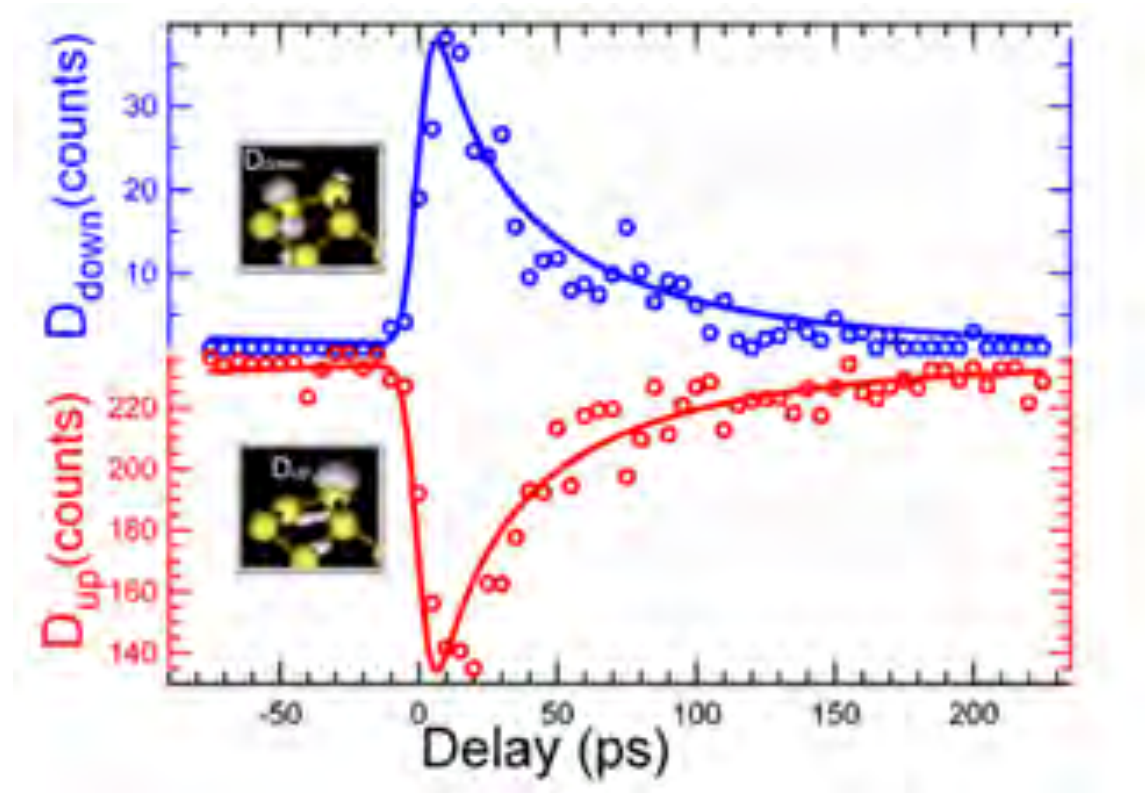


Figure 4.14: Temporal evolution of the transient population and depopulation of the D_{down} and D_{up} surface states, respectively.

dimers/cm² the carrier density created is about $3 \cdot 10^{14} / \text{cm}^2$. Therefore we expect surface recombination to contribute significantly to population and depopulation of the dangling-bond bands. From the broadening of the signal for overlapping pump and probe pulses we estimate an overall temporal resolution of 10 ps. Three processes will lead to population of the unoccupied D_{down} dangling-bond band and depopulation of its occupied counterpart D_{up}

- Direct excitation from the D_{up} to the D_{down} dangling-bond bands
- Direct excitation between D_{up} and unoccupied bulk states as well as between occupied bulk states and the D_{down} band
- Surface recombination, i.e scattering from electrons excited to the conduction band into the unoccupied dangling-bond band and scattering from holes excited in the valence-band into the occupied dangling-bond band.

Carrier transport and recombination in bulk silicon has been modeled by N. Bulgakova [Bul04]. For a fluence of 110 mJ/cm^2 at 800 nm and a pulse duration of 70 fs the density of the electron-hole plasma created is about 10^{21} cm^{-3} (for details see Section 4.4.1). The relaxation of the electron-hole population, $n_e(t)$ and $n_h(t)$, is modeled by two contributions a linear and a quadratic term:

$$\frac{dn_{e/h}}{dt} = (\alpha + \beta \cdot n_{e/h}(t)) \cdot n_{e/h}(t) \quad (4.5)$$

α describes the scattering from the surface state into defect states and is proportional to the number of excited carriers n_e or n_h , β governs the recombination between excited electron-hole pairs and is thus proportional to n_e or n_h . Solving this differential equation and assuming that the number of created holes equals the number of excited electrons, the temporal evolution of the two-dimensional electron-hole plasma in the surface bands created after laser excitation is given by:

$$n(t) = \frac{\alpha \cdot n_0}{\beta \cdot n_0 - (\alpha + \beta \cdot n_0)e^{\alpha t}} \quad (4.6)$$

For high excitation densities the dominant term is the quadratic one and by fitting the experimental data the decay time for the population of the unoccupied state and the depopulation of the occupied state was evaluated. The best fit obtained is shown in Fig. 4.14 as solid lines. We obtain $\beta = 4 \cdot 10^{11} \text{ cm}^2/\text{ps}$ and $\alpha = 1/170 \text{ ps}$. This is in good agreement with the values obtained by Bokor and coworkers [Hal89] who studied charge recombination in the surface states on the Si(111) (2×1) reconstructed surface. A decay rate of $1/170 \text{ ps}$ for electrons excited to the D_{down} dangling-bond band is also consistent with the results of M. Kutschera [Kut01] who studied single electron dynamics in the limit of low excitation fluences. For densities of $3 \cdot 10^{14} \text{ cm}^{-2}$ we obtain $\beta \cdot n = 1/2.5 \text{ ps}$ which demonstrates the dominance of the quadratic term in Eq. 4.5. From the broadening of the signal for overlapping pump and probe pulses we estimate an overall temporal resolution of 10 ps . The position of the transiently populated D_{down} band was found 0.65 eV above the D_{up} surface band. The surface band gap in the ground state is experimentally determined to 0.81 eV [Wei04]. As discussed in the next section we attribute the reduction of the surface band gap by about 0.16 eV to a renormalization of the silicon bulk gap upon laser excitation.

Bulk Contribution

The data analysis outlined in the last section allows us to separate surface from bulk contributions. Figure 4.13 illustrated the convolution of the valence-band into two Gaussian functions which represent the intensity changes of the occupied and unoccupied surface states. Moreover, the step function in Fig. 4.13 allows to quantify the change of the position of the valence-band edge upon fs laser excitation. The position of the valence-band edge is plotted in Fig. 4.15a as a function of the delay between laser and synchrotron pulses. The maximal shift observed is 220 meV. Assuming that a band-gap renormalization is almost equally distributed between the conduction and valence-bands [Osc92], the band-gap shrinks by about 400 meV.

The band-gap renormalization is caused by the carrier concentration created upon

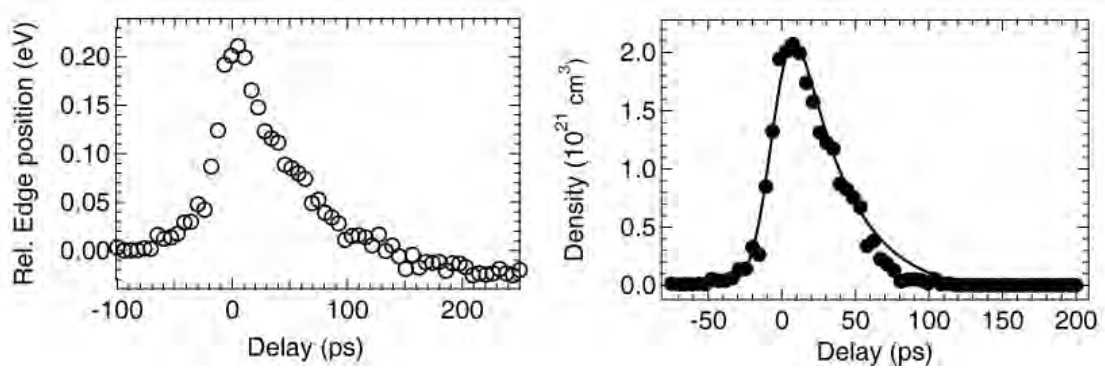


Figure 4.15: a) Temporal evolution of the position of the valence-band edge and the carrier density. b) Latter data have been extrapolated from the the calculated band-gap narrowing as a function of electron carrier concentration by Oschlies *et al.* [Osc92]. The solid line represents the fit function (Eq. 4.7) convoluted with a Gaussian of 10 ps width.

laser excitation in the bulk. Oschlies and coworkers calculated the band gap narrowing in silicon for a situation where additional electrons in the conduction band are screened by a neutralizing uniform background charge [Osc92]. Based on the calculation we can transfer the band-gap narrowing into a plasma density.

Figure 4.15b shows the temporal evolution of the carrier concentration produced upon 110 mJ/cm² infrared laser excitation. A maximum density of $2 \cdot 10^{21}$ cm⁻³ is obtained which is in excellent agreement with the already mentioned calculation by N. Bulgakova. At high carrier densities Auger recombination is sufficiently fast to ensure that electrons and holes rapidly reach a quasiequilibrium with the lattice by thermalization of hot electrons. Specifically, in the Auger process an electron recombines with a hole and the released energy is taken up by a third carrier. This hot carrier will rapidly thermalize as indicated in Fig. 4.16b. Primary channels for energy relaxation of the hot carriers are collisions between carriers, plasmon production

and phonon emission. The relaxation via Auger decay follows the relation [Yof80]:

$$\frac{dn}{dt} = -C_{eh}n^3 \quad (4.7)$$

where C_{eh} is the Auger coefficient for e-e-h and e-h-h scattering processes. From the fit of the data in Fig. 4.15b we obtain an Auger coefficient of $C_{e-h}=6.4 \cdot 10^{-33} \text{ cm}^6\text{s}^{-1}$. This value is about one order of magnitude larger than experimentally [Dow86] and theoretically [Yof80] determined values for bulk silicon. This discrepancy is not considered significant, since the third power of the carrier concentration enters Eq. 4.7 and its evaluation from the band-gap narrowing may certainly account for the error.

N. Bulgakova simulated the transport and recombination of excited carriers in

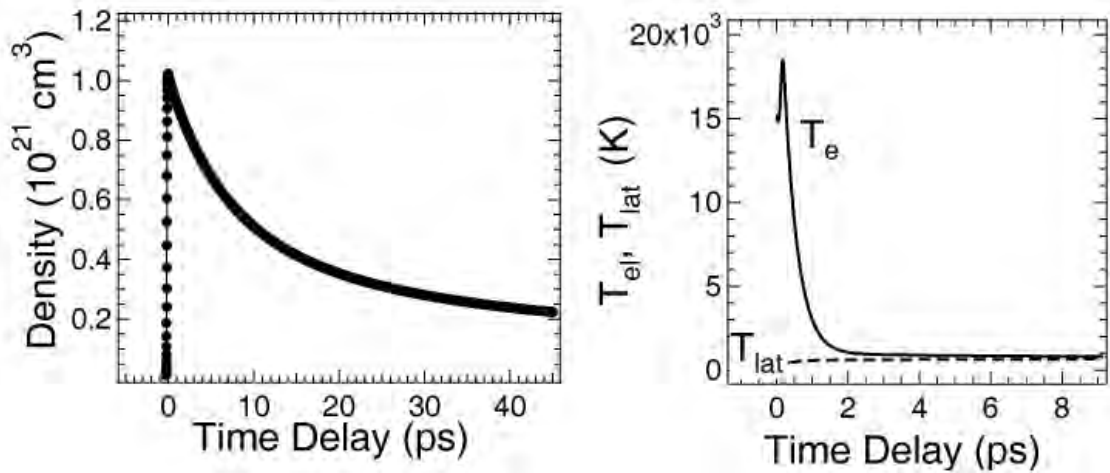


Figure 4.16: a) Temporal evolution of free-electron population. Excitation by a 800 nm, 80 fs pulse width and a laser excitation of 110 mJ/cm². b) The electron and lattice temperature profiles.

silicon for different fluences of femtosecond laser excitation. Assuming that density and temperature gradient lead to diffusion but charge separation and the generated electric field do not cause electrons and holes to travel separately, diffusion and drift of carriers is described selfconsistently [Bul04, Bul05]. The calculated transient carrier density is shown in Fig. 4.16a. As already mentioned, the calculated maximum carrier density for a fluence of 110 mJ/cm² is about 10²¹ cm⁻³ and thus in good agreement with the estimate from the silicon band-gap narrowing. The decay of the population is mainly determined by the Auger recombination (c.f Eq. 4.7).

Figure 4.16b shows the electron and lattice temperature profiles. Hot electrons created by a 110 mJ/cm² excitation pulse are thermalized in one picosecond. The lattice and the electronic temperatures are almost constant during the following picoseconds and the temperature of the system has to be described by two slightly different temperatures. Equilibration between carriers and lattice is now governed

by the relatively slow Auger decay process. This leads to a lifetime of the excited carriers of several tenths of picoseconds.

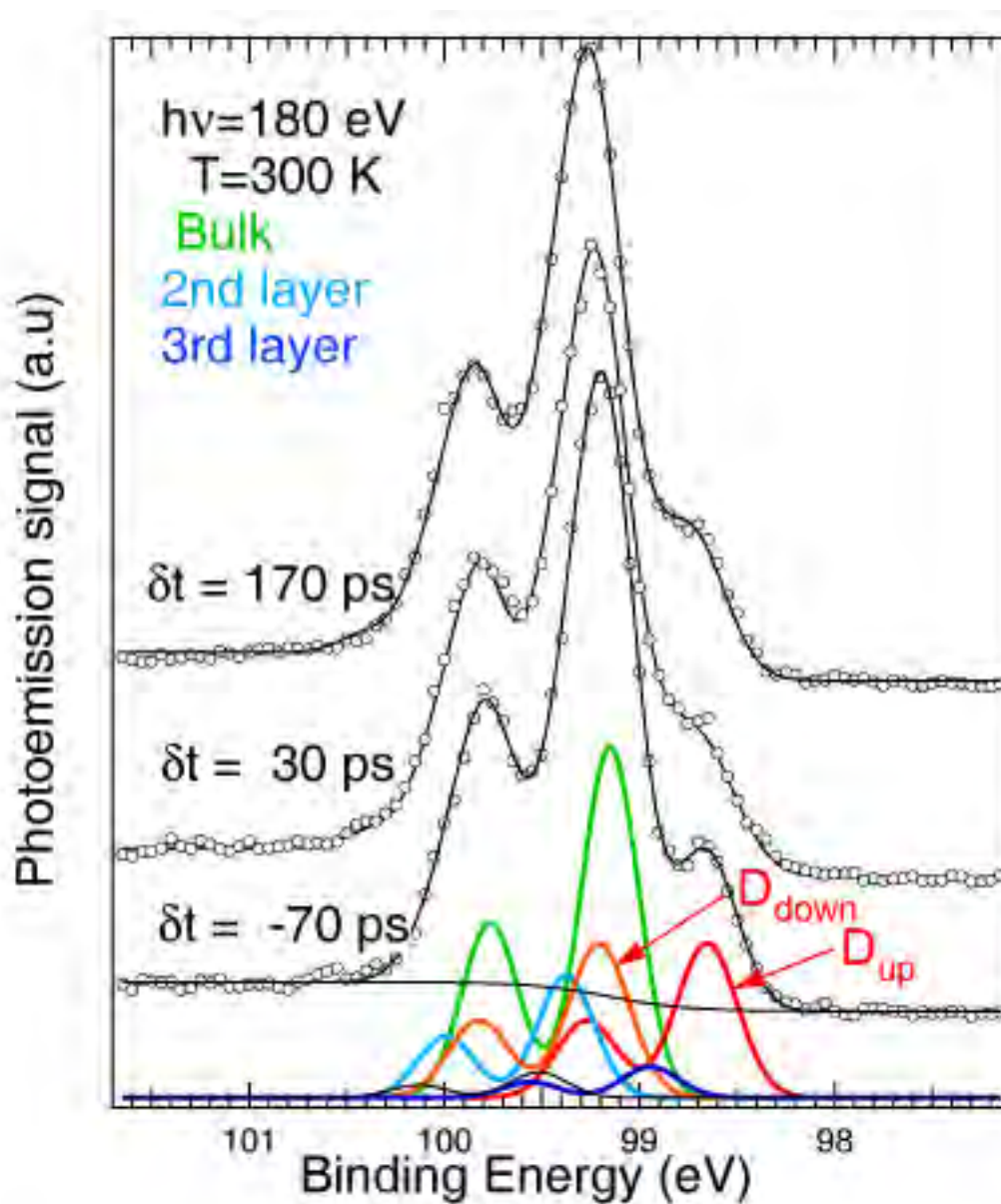


Figure 4.17: Si 2p spectra recorded under similar conditions as the valence-band spectra in Fig. 4.13 for three different time delays between laser and synchrotron pulses. The Si 2p spectrum was deconvoluted by seven double Gaussian functions, and a broadened step function for the background of secondary electrons [Koh03].

4.4.2 Core-Level Dynamics

Figure 4.17 shows the Si 2p core-level spectra of Si(100) for three different time delays between laser and synchrotron measured with the same experimental conditions as the valence-band spectra except for the laser fluence. The laser fluence used for time-resolved experiments at the Si 2p core-level was 40 mJ/cm^2 . At higher laser fluences the splitting between Si $2p_{3/2}$ and Si $2p_{1/2}$ components disappears due to space charge effects (see Section 4.4.3). The deconvolution of the different contributions to the Si 2p core-level are indicated in Fig. 4.17. The surface contribution is located at higher binding energies and the bulk contribution is located at lower binding energies. The spectra shows a transient broadening of the surface component upon laser excitation while the bulk component is little affected. The feature at lower binding energy representing the D_{up} surface components broadens significantly more than the feature at higher binding energy bulk component (see Fig. 4.17).

The Si 2p spectra are deconvoluted following the assignment of the spectral features by Koh *et al.* [Koh03], who measured Si 2p spectra at different photon energies with high energy resolution. According to their analysis the Si 2p core level spectra consist of seven spin-orbit split components, which are shifted with respect to each other and are assigned to electrons excited from the Si 2p core-level of the upper and lower surface dimer atoms, the atoms of the second and third layer, bulk atoms and atoms located at crystal defects. Independent parameters are the position of the Si 2p, its intensity and the Gaussian width of the surface and bulk components. The rest of the parameters have been fixed according to Koh *et al.* [Koh03] in order to simplify the analysis. At the bottom in Fig. 4.17 the fit function of the Si 2p spectrum is plotted, which consist of a set of seven Gaussian functions and a broadened step function for the background of secondary electrons. Each double Gaussian function of the fit function describes the contribution of surface, bulk, second layer, third layer and defect states. The widths of all Gaussian peaks except the surface component is equal and the amplitude ratio between the Si $p_{3/2}$ and the Si $p_{1/2}$ are constrained to be close to 2, thereby further reducing the number of free parameters. Before further analyzing the transient broadening of the core-level spectra we first discuss the influence of the pump pulse intensity.

4.4.3 Damage threshold and Multiphoton Ionization at the Si(100) Surface

The damage threshold of silicon was experimentally determined to 180 mJ/cm^2 . This value is in good agreement with previous theoretical [Bul04, Bul05] and experimental [Jes02] studies.

Figure 4.18 shows Si 2p spectra recorded for different delays between laser and

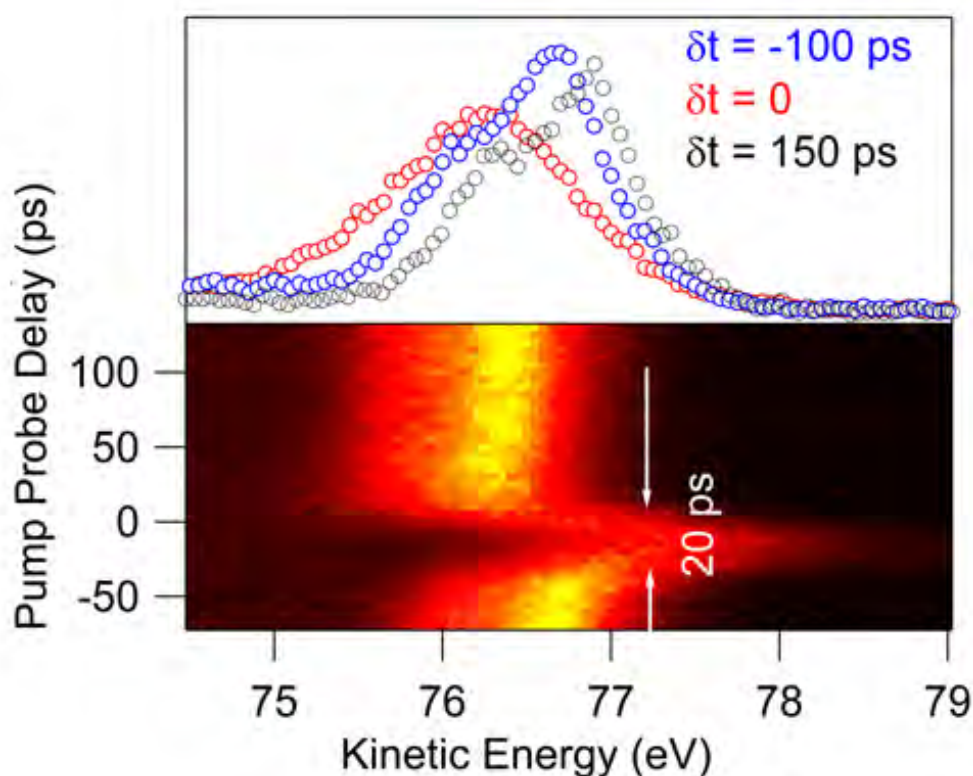


Figure 4.18: Top: Si 2p spectra for delay between laser and synchrotron pulses, negative (blue-spectrum), positive (black-spectrum) and close to zero (red-spectrum). Bottom: Two dimensional plot, delay between laser and synchrotron versus kinetic energy

synchrotron pulses at a laser fluence of 180 mJ/cm^2 . A significant loss of intensity in the surface core-level component of the Si 2p spectra was used as criterium for the damage threshold. The spot irradiated by the laser shows irreversible changes in the Si 2p core-level and a further analysis of the set of data recorded for a laser fluence of 180 mJ/cm^2 was not possible due to these changes. The Si 2p core-level has to be measured at lower laser excitation fluence.

The value of damage threshold depends on the material, the absorbed energy, the optical excitation fluence and the photon energy. The irreversible changes at the surface occur when a critical electron density is reached, where resonant collective electronic oscillations break broking bonds and lead to desorption of single silicon atoms from the clean silicon surface.

Figure 4.19 illustrates the multiphoton process produced by the laser itself (solid-line). The probe photon-energy of the synchrotron-radiation was chosen in order to attenuate the contribution of photoelectrons excited by multiphoton processes to the valence-band and core-level spectra. The dotted-line shows the Si 2p spectrum measured for a laser fluence of 60 mJ/cm^2 i.e well below the damage threshold. The

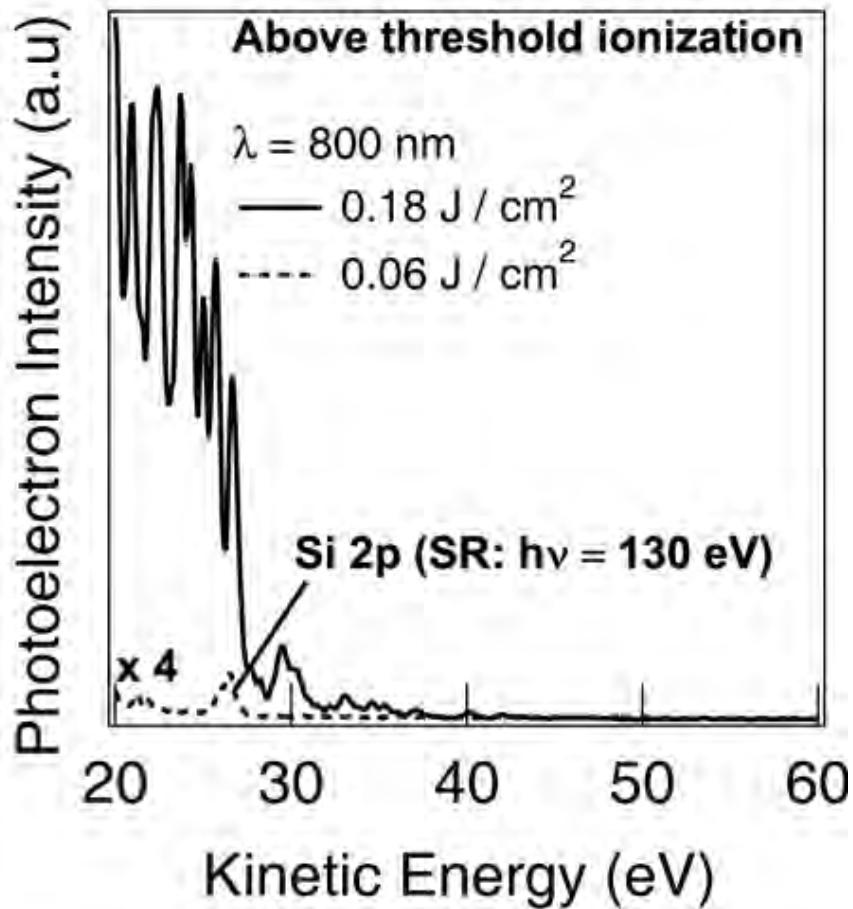


Figure 4.19: Multiphoton processes produced by the laser pulse (solid-line) for an excitation fluence of 180 mJ/cm^2 . The dot line represents the Si 2p spectrum measured with laser and synchrotron pulses for a laser excitation fluence of 60 mJ/cm^2 .

photon-energy of the synchrotron probe-pulse was chosen to avoid overlap with the multiphoton process leading to photoemission at lower kinetic energy.

Figure 4.20 plots the result of the simulation performed by N. Bulgakova for a laser excitation fluence of 180 mJ/cm^2 . Figure 4.20a presents the temporal evolution of the electron-hole plasma-density created for a laser fluence of 180 mJ/cm^2 . Figure 4.20b presents the evolution of the electrons and lattice temperature. The electronic system cools down in about 20 ps but the complete thermalization with the lattice requires more than hundred nanoseconds.

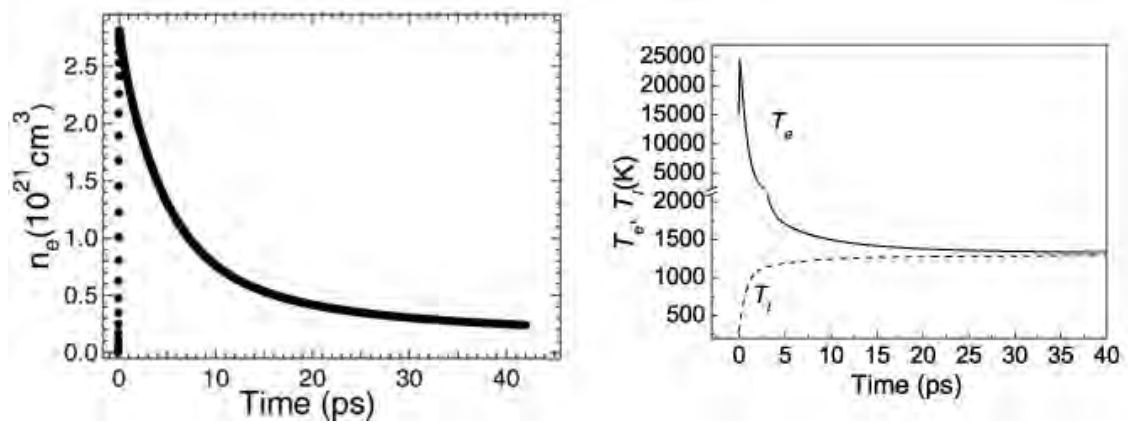


Figure 4.20: a) The electron T_e and lattice temperature T_l profiles. b) Temporal evolution of free electron population. Both calculated for a 800 nm, 80 fs pulses at a laser excitation fluence of 180 mJ/cm^2 .

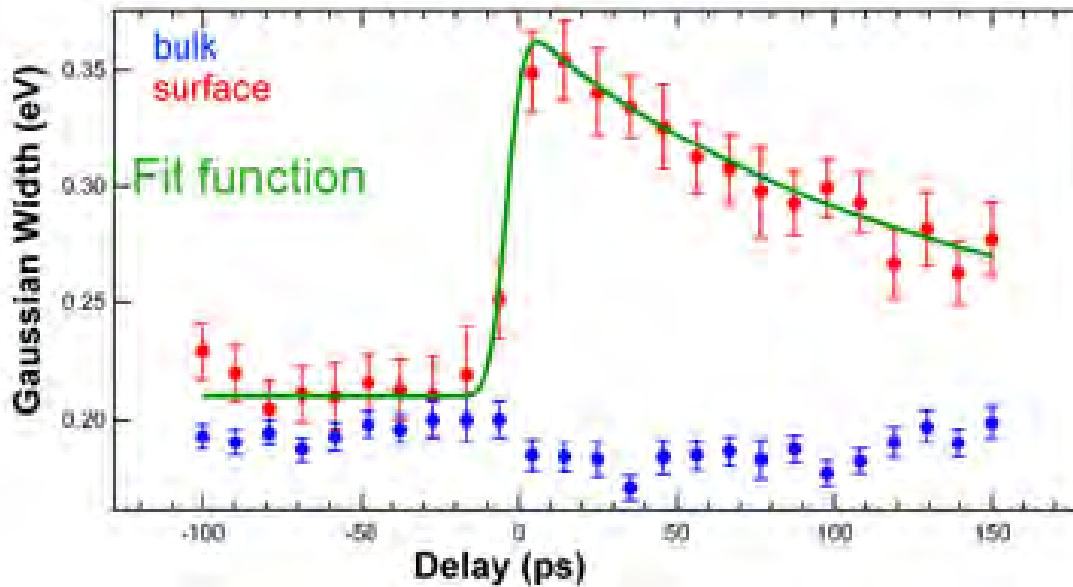


Figure 4.21: Results of an analysis of the Si 2p spectra reproduced in Fig. 4.17. The surface components (red) are broadened upon laser irradiation by approximately 140 meV, while the width of the remaining components stays nearly constant. The solid green line is a fit as described in the text.

4.4.4 Transient Broadening of the Surface Core-Level

As evident from the previous chapter the transient broadening of the Si 2p core-level can only be analyzed for moderate laser fluence, where space charge effects due to multiphoton process are substantially suppressed. For a fluence of 40 mJ/cm^2 the transient broadening of the Si 2p core-level is plotted in Fig. 4.21. The assignment

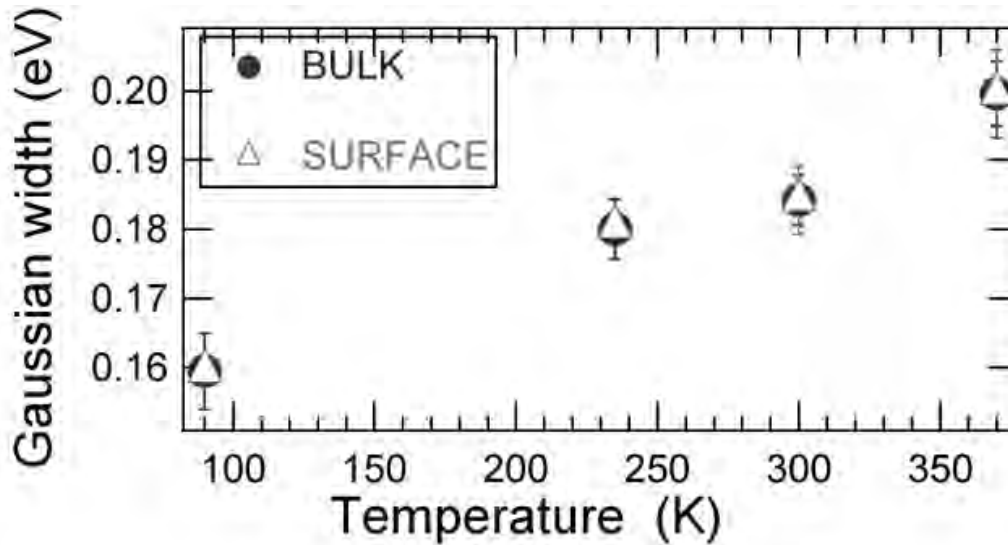


Figure 4.22: Surface (red-dot) and bulk (blue-dot) peak width as function of silicon sample temperature during thermal annealing.

of the surface and the bulk Gaussian widths is done following the analysis described in Section 4.4.2 and illustrated in Fig. 4.17. The surface components broaden by 140 meV while the width of the remaining components stays nearly constant. What causes the transient broadening of the surface component, lasting for several tenths of picoseconds?. A simple temperature effect which induces a different broadening of surface and bulk components can be rule out by static measurements of Si 2p spectra at different temperatures. As depicted in Fig. 4.22 where the bulk and surfaces components broaden proportional with the temperature.

Figure 4.23a and b show again calculations of carriers density and electron and lattice temperatures for an excitation fluence of 40 mJ/cm² and a 800 nm laser pulse of 80 fs duration. For this excitation density the carriers density in the bulk decays rather slowly and will support a long lasting population of the dangling-bond band via surface recombination.

Furthermore, the lattice temperature increases only from 300 to 350 K within the first 3 ps after laser excitation. Thus a temperature induced broadening of the Si 2p surface component is rather unlikely. As corroborated by static measurements of the Si 2p core-level at different temperatures. As depicted in Fig. 4.22 we find a comparable broadening of both the surface and the bulk components.

Therefore, it seems evident that the broadening of the surface component is surface specific and likely a signature of a variation of the dimer buckling angle. As show in Section 4.4.1 upon laser excitation the occupied dangling-bond band D_{up} becomes depopulated, while the unoccupied dangling-bond band D_{down} is transiently populated. The splitting of the dangling-bond states in occupied and unoccupied

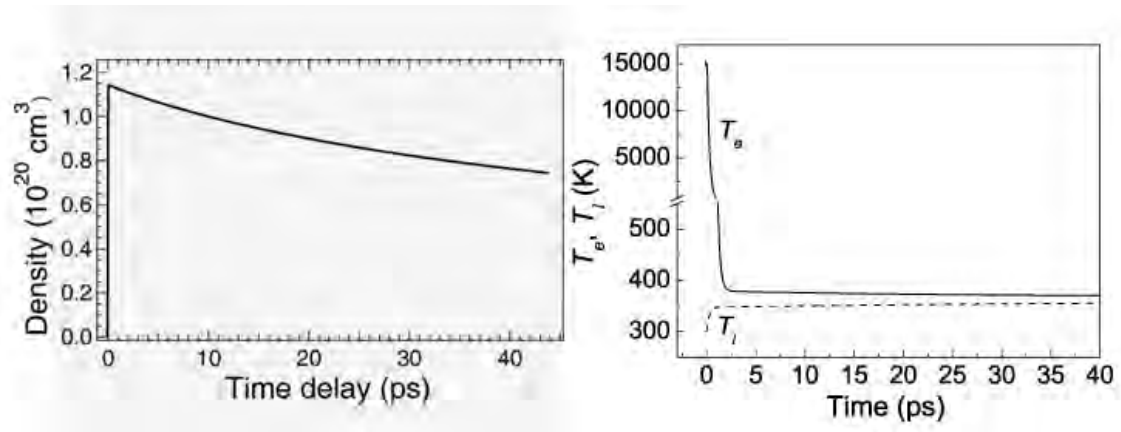


Figure 4.23: a) Temporal evolution of free electron population. b) The electron and lattice temperature profiles. Both by a 800 nm, 80 fs pulse width and a laser excitation of 40 mJ/cm^2 .

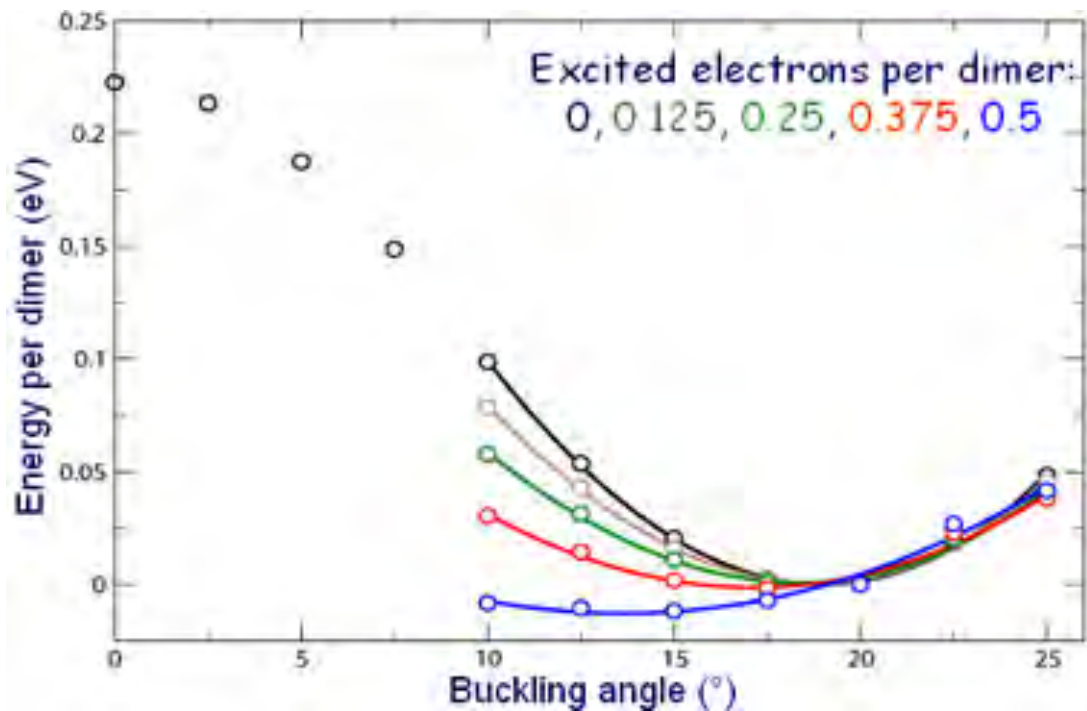


Figure 4.24: Calculation from excitation energy pro dimer as a function of the dimer buckling angle.

bands is, however, intimately connected to the tilt angle of the dimer. This may be seen from a comparison of the symmetric and asymmetric dimer model. Density functional theory (DFT) predicts that in the AMD the surface is semiconducting while in the SMD the silicon surface is metallic. This may be understood as a Peierls

distortion where the opening of a gap in the electronic structure is closely related with a distortion of the lattice. Upon laser excitation we created holes in the D_{up} band and electrons in the D_{down} band and the surface become metallic. Therefore, we expect in response a change in the tilt angle of the dimer. This simple model is confirmed by DFT calculation from van Hei and Pehlke [Peh06]. Figure 4.24 shows the energy per dimer as a function of the dimer buckling angle for an array of silicon slabs with 16 layers. In the ground state the minimum energy yields a tilt angle of about 18° in close agreement with experimental findings. Upon charge redistribution the potential softens. For half an electron excited per (2×1) unit cell the potential is very flat. As many tilt angles are now energetically possible, we expect a significant inhomogeneous broadening of the surface core-level components. Further evidence for this interpretation stems from the delay dependence of the transient broadening. The data in Fig. 4.21 have been fitted by Eq. 4.6, with the values α and β derived from the population dynamics in the D_{up} and D_{down} dangling-bond states.

The overall agreement between fit (solid green line) and data suggests that the broadening of the surface component is induced caused by the transient charge redistribution at the surface. The excited carriers stay for picoseconds and stabilize a new transient structure.

